American Mineralogist, Volume 93, pages 853–862, 2008

Crystal chemistry of the natrojarosite-jarosite and natrojarosite-hydronium jarosite solid-solution series: A synthetic study with full Fe site occupancy

LAUREL C. BASCIANO* AND RONALD C. PETERSON

Department of Geological Sciences and Geological Engineering, Queen's University, Kingston, Ontario, Canada

ABSTRACT

Members of the natrojarosite-hydronium jarosite [$(Na,H_3O)Fe_3(SO_4)_2(OH)_6$] and jarosite-natrojarosite [$(K,Na)Fe_3(SO_4)_2(OH)_6$] solid-solution series were synthesized and investigated by Rietveld analysis of X-ray powder diffraction data. The synthesized samples have full Fe occupancy, where in many previous studies there were significant vacancies in the B site. Well-defined trends can be seen in the unit-cell parameters across the solid-solution series in the synthetic samples. The majority of the samples in this study were directly synthesized under hydrothermal conditions at 140 °C. End-member natrojarosite was synthesized using a two-step method, where the initial sample was heated in a 1.0 *m* H_2SO_4-0.5Na_2SO_4 solution at 200 °C for 3 days, yielding a sample with 100% Na occupancy. Many of the samples were initially zoned and required grinding and re-heating in the reactant solution for homogenization. Substitution of H_3O and K into natrojarosite changes unit-cell parameters in a linear fashion. The unit-cell parameters presented here are significantly different than the majority of previous studies on synthetic samples, as samples in the current study have full Fe occupancy and the Na-K jarosite series has no H_3O substitution in the A site. Substitution in the A site mainly affects unit-cell parameter *c* with little change in *a*. As Na occupancy increases there is a decrease in A-O2 and A-O3 distances and a consequent increase in Fe-O2 and Fe-O3 distance leading to an overall decrease in unit-cell parameter *c* in both the Na-H_3O and Na-K jarosite series. The synthetic samples are compared to natural samples from mine waste deposits in Rio Tinto (Huelva, Spain), Ely Mine (Vermont), and a mineral collecting locality near Sharbot Lake (Ontario), as well as natural and synthetic samples documented in the literature. Based on unit-cell parameters many of the natural samples appear to have full Fe occupancy and correlate well with the synthetic samples from this study. The infrared spectra of the samples were analyzed, and there is a gradual change in the spectral features across the solid-solution series between end-members. The results from this study will aid in the interpretation of the possible chemical compositions of natural jarosite group minerals in mine waste and on Mars.

Keywords: Jarosite, hydronium jarosite, natrojarosite, solid-solution series, crystal synthesis, crystal structure, IR spectroscopy, Rietveld refinement

INTRODUCTION

The jarosite group of minerals is part of the alunite supergroup, which consists of 40 mineral species that have the general formula $AB_3(TO_4)_2(OH)_6$. There is extensive solid solution in the A, B, and T sites within the alunite supergroup, where A may be occupied by H_3O^+, Na^+, K^+, Rb^+, Ag^+, Tl^+, NH^{4+}, $\frac{1}{2}Ca^{2+}$, or $\frac{1}{2}Pb^{2+}$, B may be occupied by Fe^{3+} or Al^{3+} and TO_4 may be SO_4^{2-}, PO_4^{3-}, or AsO_4^{3-} (Scott 1987; Stoffregen and Alpers 1987). The jarosite group is characterized by B = Fe^{3+} and T = S. Jarosite (A = K) and natrojarosite (A = Na) are the most prevalent naturally occurring jarosite group minerals and hydronium jarosite is rare, though most jarosite group minerals contain some hydronium in the A site (Ripmeester et al. 1986; Drouet and Navrotsky 2003; Majzlan et al. 2004). Hydronium jarosite will only form in alkali-deficient solutions, as alkali-rich jarosite forms preferentially. For the sake of clarity, jarosite, sensu stricto, will be referred to as K jarosite throughout this paper.

The jarosite group of minerals has been extensively studied as a result of its importance as a by-product of the metal-processing industry as well as being a common supergene mineral in ore deposits, and its association with acid-mine waste. Minerals within the jarosite group are commonly found in acidic, high-sulfate environments. In mine waste, metal-rich acidic waters originate from the oxidation of sulfide minerals, such as pyrite (FeS_2). Jarosite is thought to exist on Mars, and its presence suggests that water existed on Mars in the past (Klingelhöfer et al. 2004; Madden et al. 2004; Papike et al. 2006a, 2006b). The position of Fe^{3+} ions in the jarosite structure may be described by a Kagomé lattice, and the magnetic properties have led to additional research in this area (Wills and Harrison 1996; Greedan 2001; Grohol et al. 2003; Harrison 2004; Nocera et al. 2004; Bartlett and Nocera 2005). The jarosite group is thought to be the principle model for studying spin frustration. The Kagomé layers are formed from the corner-sharing Fe_3^{3+}-(μ-OH)$_3$ triangles and are the most highly geometrically frustrated two-dimensional lattice (Bartlett and Nocera 2005).

Synthetic and natural members of the jarosite group often

* E-mail: basciano@students.geol.queensu.ca

have vacancies in the B site with Fe site occupancies as low as 86%. Non-stoichiometry in the B site has been studied by Hendricks (1937), Kubisz (1970), Ripmeester et al. (1986), Drouet and Navrotsky (2003), Grohol et al. (2003), Drouet et al. (2004), and Basciano and Peterson (2007). Additionally, there is often substantial substitution by hydronium for Na or K in the A site. Iron deficiency in the B site leads to a decrease in unit-cell parameter *c* and hydronium substitution increases unit-cell parameter *a*. Many synthetic samples in the literature exhibit the effects of Fe deficiency and hydronium substitution. Jarosite with fully occupied B sites have been synthesized by Grohol and Nocera (2002), Grohol et al. (2003), and Basciano and Peterson (2007). The presence or absence of H_3O^+ in alunite and jarosite group structures has been extensively discussed in the literature (Nielson et al. 2007; Drouet and Navrotsky 2003; Kubisz 1970; Dutrizac and Kaiman 1976; Ripmeester et al. 1986). The orientation of the hydronium group has not been determined reliably in either X-ray diffraction or neutron diffraction studies (Lager et al. 2001; Majzlan et al. 2004; Nielson et al. 2007) as the molecule is dynamically disordered. The commonly noted cation deficiency in the A site has been assumed in the majority of studies to be the result of hydronium substitution. Majzlan et al. (2004) and Basciano and Peterson (2007) found that the A site is not fully occupied in end-member hydronium jarosite, with the occupancy of oxygen in the A site being 91 and 92%, respectively. In these cases, it is probable that charge neutrality is maintained by protonation of OH^- to form OH_2 (Majzlan et al. 2004). Recently, Nielson et al. (2007) reinvestigated structural defects in the structure of natural and synthetic alunites with multi-nuclear solid-state NMR spectroscopy, including B site deficiencies and hydronium substitution in the A site. They found that the hydronium ion (H_3O^+) was observed in hydronium alunite but was not detected in the spectra of alunite and natroalunite that had less than 100% A site occupancy of K or Na. They suggest that an Al vacancy at the B site is compensated by the addition of 4 H^+. H_3O^+ in the A site is then not necessary for charge balance, resulting in the A site vacancy that is commonly seen.

The solid-solution series among the Na-, K-, and H_3O-jarosite end members have been studied previously by Brophy and Sheridan (1965), Brown (1970), Kubisz (1970, 1972), Dutrizac (1983), and Drouet and Navrotsky (2003). The B sites in the synthesized jarosite members in these previous studies were not fully occupied with Fe, resulting in smaller unit-cell parameters. Unit-cell parameters of members of the Na-K jarosite solid-solution series were plotted in Stoffregen et al. (2000) from unpublished data. The crystal structure of natrojarosite has not been studied in detail previously. Grohol et al. (2003) reported the structure of stoichiometric natrojarosite in a study relating to the magnetic properties of jarosite. There are differences between the unit-cell parameters reported in that study and those reported here.

EXPERIMENTAL METHODS

Sample synthesis

The solid-solution series $(H_3O)_{1-x}Na_xFe_3(SO_4)_3(OH)_6$ was synthesized using the same method as in Basciano and Peterson (2007). Samples were synthesized hydrothermally in stainless steel vessels at 140 °C for 48 h. Synthesis conditions are summarized in Table 1. Forty grams of ACROS brand $Fe_2(SO_4)_3 \cdot 5H_2O$ and varying amounts of Fisher Scientific Na_2SO_4 (0–1.0 g) were mixed with deionized water to a volume of 100 mL at room temperature. These conditions were used to ensure a high concentration of Fe^{3+} ions in solution. Low relative concentration of Fe^{3+} ions in the starting solutions resulted in deficiency of Fe in synthesized jarosite (Kubisz 1970). During the H_3O-Na jarosite solid-solution synthesis, it was noted that below ~50% Na in the final product there was some peak broadening, indicating non-homogeneity of the samples similar to results found in Basciano and Peterson (2007) for the K jarosite-hydronium jarosite solid-solution series. In samples where there was peak broadening, samples were finely ground in a McCrone Micronizing Mill with deionized water after the initial synthesis and re-heated at 140 °C in the reactant solution. Samples were analyzed after three days of heating using XRD to determine sample homogeneity. All samples were homogenized after two cycles of annealing, based on achieving sharp peaks in XRD spectra of the annealed samples.

The solid-solution series $(Na)_{1-x}K_xFe_3(SO_4)_3(OH)_6$ was synthesized in a chloride-rich medium using a method similar to that of Frost et al. (2005). It was found that the high-chloride concentration reduced the amount of hydronium entering the structure. Five milliliters of 1.23 *M* $FeCl_3$ solution, and a 0.5 g mixture of NaCl and KCl were dissolved in 12 mL concentrated LiCl solution. Six grams of $Fe(SO_4)_3 \cdot 5H_2O$ was dissolved in 25 mL deionized water and slowly added to the chloride solution. The final solution was heated for 48 h in a stainless steel pressure vessel at 140 °C. All samples had varying amounts of peak widening during preliminary X-ray analysis. As in the K-hydronium jarosite solid-solution series (Basciano and Peterson 2007), K jarosite precipitated out of solution first, followed by natrojarosite. The samples were ground in a McCrone Micronizing Mill and annealed in the reactant solution until the sample was homogeneous based on XRD spectra.

End-member natrojarosite with the A site fully occupied with Na was not grown using the two above methods as some hydronium remains in the structure. Fully occupied natrojarosite was grown using a two-step method similar to Stoffregen (1993). Natrojarosite with ~87% Na occupancy was first grown using the same method outlined above for the Na-H_3O jarosite series and then ground in a McCrone Micronizing Mill. The sample was then heated in a 1.0 *m* H_2SO_4-0.5Na_2SO_4 solution at 200 °C for 3 days in a Parr pressure vessel, which yielded an A site occupancy of 100% Na as determined by ICP-OES and normalized to 2 S per formula unit.

Atomic structural parameters for end-member K jarosite and hydronium jarosite were taken from Basciano and Peterson (2007).

X-ray powder diffraction and Rietveld refinement

Powder-diffraction data were collected from 15–100 °2θ (Fe filtered Co*K*α radiation) from a back-packed sample using a Panalytical X'Pert theta-theta diffractometer and an X'celerator position-sensitive detector equipped with incident- and diffracted-beam soller slits, and ½° divergence and 1° anti-scatter slits. The normal-focus Co X-ray tube was operated at 40 kV and 45 mA. Profiles were taken with a step interval of 0.008 °2θ, and an effective counting time per step of 30 s. To eliminate preferred orientation, samples were ground for 2 min in a McCrone Micronizing Mill in water and backpacked against a 320-grit sandpaper surface. The data were refined with the Rietveld refinement program Topas Academic (Coelho 2004). Starting atomic parameters were taken from Majzlan et al. (2004). The instrument parameters were modeled using a full axial divergence model defined by Cheary and Coelho (1998). Co*K*α source emission profiles were taken from Hölzer et al. (1997). Broadening due to crystallite size was refined using the Double-Voigt approach (Balzar 1999). Sodium and potassium occupancy in the A position were set to the occupancy determined with ICP-OES and the T site is assumed to be fully occupied by S. Starting hydrogen positions (OH group) were taken from the single-crystal study of hydronium jarosite by Majzlan et al. (2004) and were restrained at 0.8 Å. The O-H bond length was restrained at 0.8 Å instead of 0.98 Å, which is the average O-H bond length in crystalline solids refined by X-ray diffraction (Baur 1972), because observed O-H distances in X-ray determinations tend to be on average 0.2 Å shorter than in neutron diffraction (Baur 1972). The displacement parameters of the H atoms were fixed at 2 and not refined.

The data collection and structure refinement details are given in Table 2. A final Rietveld refinement plot of observed and calculated intensities for end-member ammoniojarosite is shown in Figure 1.

Short-wave infrared reflectance spectroscopy (SWIR) and mid-infrared analysis (MIR)

Short-wave infrared reflectance spectra of the synthetic Na-H_3O and Na-K jarosite solid-solution series were collected using a Portable Infrared Mineral Analyzer (PIMA), Integrated Spectronics SP instrument, which measures in the 1200–2600 nm range. Mid-infrared-absorption spectra of the synthetic samples were collected using a Nicolet Avatar 320 Fourier Transform Infrared Spectrometer

TABLE 1. Chemical compositions of starting solutions and synthetic jarosite samples

	Starting solution compositions (g)		Analytical results (ICP-OES) (% occupancy) and formula				
Synthetic samples	$Na_2(SO_4)$	$K_2(SO_4)$	Fe%	K%	Na%	S%	Formula
K	0.05	0.45	100.2	77.6	25.6	100	$(K_{0.78}Na_{0.26})Fe_{3.01}(SO_4)_2(OH)_6$
L	0.10	0.40	104.7	60.9	41.5	100	$(K_{0.61}Na_{0.41})Fe_{3.14}(SO_4)_2(OH)_6$
M	0.25	0.25	102.5	52.2	46.1	100	$(K_{0.52}Na_{0.46})Fe_{3.08}(SO_4)_2(OH)_6$
N	0.40	0.10	98.5	28.8	69.5	100	$(K_{0.29}Na_{0.69})Fe_{2.95}(SO_4)_2(OH)_6$
O	0.45	0.05	98.8	11.1	85.0	100	$(K_{0.11}Na_{0.85})Fe_{2.96}(SO_4)_2(OH)_6$
P*	na	na	102.0	–	97.7	100	$(Na_{1.0}\ H_3O_{0.0})Fe_{3.06}(SO_4)_2(OH)_6$
Q	0.85	–	98.8	–	87.5	100	$(Na_{0.87}H_3O_{0.13})Fe_{2.96}(SO_4)_2(OH)_6$
R	0.70	–	98.3	–	68.6	100	$(Na_{0.67}H_3O_{0.33})Fe_{2.95}(SO_4)_2(OH)_6$
S†	1.0	–	103.8	–	49.4	100	$(Na_{0.49}H_3O_{0.51})Fe_{3.11}(SO_4)_2(OH)_6$
T†	0.6	–	99.8	–	35.0	100	$(Na_{0.35}H_3O_{0.65})Fe_{2.99}(SO_4)_2(OH)_6$
U†	0.2	–	99.4	–	23.8	100	$(K_{0.24}H_3O_{0.76})Fe_{2.98}(SO_4)_2(OH)_6$

Note: Chemical analyses are based on 2 S per formula unit.
* Synthesized in chloride media similar to Frost et al. (2005), see text for details.
† Samples were not annealed as there was no evidence of peak broadening.

TABLE 2. Data collection and structure refinement details

			K jarosite-natrojarosite $R\bar{3}m$				
Sample	I*	K	L	M	N	O	P
(Na,K)	(0.0,0.95)	(0.26,0.78)	(0.41,0.61)	(0.46,0.52)	(0.69,0.29)	(0.85,0.11)	(1.0,0.0)
a (Å)	7.30293(8)	7.3045(1)	7.3052(2)	7.3079(2)	7.3101(1)	7.3144(1)	7.31525(6)
c (Å)	17.2043(2)	17.0875(3)	16.9706(6)	16.9028(4)	16.7658(4)	16.6491(2)	16.5868(2)
V (Å^3)	794.62(2)	789.57(3)	784.32(5)	781.76(4)	775.90(3)	771.40(3)	768.69(1)
R_p	3.289	3.932	4.179	7.037	6.431	3.561	4.498
R_{wp}	4.288	6.124	6.525	10.754	9.861	5.190	5.896
R_{exp}	3.570	3.394	3.376	4.631	4.545	3.200	4.946
S	1.201	1.805	1.933	2.322	2.170	1.622	1.192
D-W	0.745	0.346	0.293	0.209	0.241	0.430	0.754

			Natrojarosite-hydronium jarosite $R\bar{3}m$			
Sample	Q	R	S	T	U	A*
Na	0.87	0.67	0.49	0.35	0.24	0.00
a (Å)	7.31984(9)	7.3254(1)	7.33876(9)	7.3420(2)	7.34742(9)	7.3552(2)
c (Å)	16.6474(2)	16.7209(3)	16.8105(2)	16.8574(4)	16.9253(2)	16.9945(4)
V (Å)	772.47(2)	777.07(3)	784.07(2)	786.95(4)	791.29(2)	796.21(4)
R_p	3.077	4.943	5.040	3.131	3.549	3.571
R_{wp}	4.188	7.099	6.801	4.356	4.651	4.773
R_{exp}	3.166	4.405	4.902	3.124	3.904	3.882
S	1.323	1.612	1.387	1.395	1.191	1.230
D-W	0.623	0.424	0.554	0.547	0.740	0.691

Notes: Step range (°2θ) 15–100°, step interval 0.008. R_p = R-pattern, R_{wp} = weighted-pattern, R_{exp} = *R*-expected, S(=R_{wp}/R_{exp}) = Goodness of fit (Young 1993). D-W = Durbin-Watson *d*-statistic (Hill and Flack 1987).
* K jarosite from Basciano and Peterson (2007). Note: A site occupancy determined with ICP-OES.

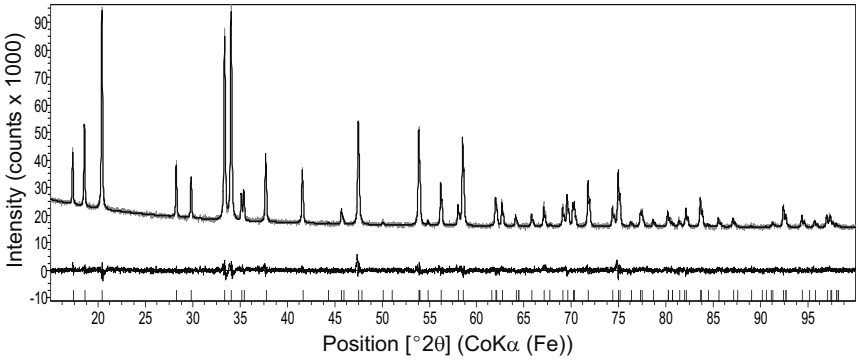

FIGURE 1. Rietveld refinement plot of sample P, natrojarosite. The gray line is the observed data and the solid line is the calculated pattern. The vertical bars mark all possible Bragg reflections (Co$K\alpha_1$ and $K\alpha_2$). The difference between the observed and calculated patterns is shown at the bottom.

and a Golden Gate diamond ATR. Spectra were measured from 400–4000 cm^{-1}. Spectral measurements were obtained from finely ground powders created for X-ray powder diffraction and Rietveld refinement.

Chemical analysis

The Fe, K, Na, and S content of the solid jarosite samples were determined using a Varian Vista CCD Simultaneous ICP-OES at Analytical Services Unit, Queen's University. The samples were digested in aqua regia and diluted for analysis. The average analytical accuracy and precision for each element is: Fe ±2%, 4.1%; Na ±6%, 5.2%; K ±5%, 4.7%; and S ±2%, 5.3%. From these data the occupancy of the alkali and Fe sites were determined in the solid samples based on the ratio of alkali and Fe to S. The mol% K, Na, and Fe in these sites were normalized to two S atoms per chemical formula based on the ideal jarosite chemical formula in which the sulfate tetrahedron is fully occupied by S. The chemical compositions of synthetic samples are given in Table 1.

Natural samples

Natural supergene samples were collected from the San Miguel mine in the Rio Tinto mining area in Spain, Ely Mine in Vermont, and from near Sharbot Lake in Ontario. Only a small number of samples from each area were analyzed using Rietveld refinement as others were a mixture of many minerals. The Rio Tinto mining district is part of the Iberian Pyrite Belt (IPB), which is host to massive and stockwork pyrite ore bodies containing base and precious metals such as Cu, Pb, Zn, Au, and Ag. The IPB has been mined using both opencast and underground mining methods, from ~2500 BC to the present day (Hudson-Edwards et al. 1999). Ely mine is part of the Vermont copper belt, which has been mined from 1793 to 1958. Ely and associated mines are Besshi-type massive sulfide deposits that are enriched in Cu as well as Zn, Ag, and Au. The sample from Sharbot Lake was collected from a cut of an abandoned railroad in the southern part of the town of Sharbot Lake, Ontario. The sample was found in a 5 mm vug in a silicicious rock sample taken from the railroad cut. The sample location was a dravite mineral collection locality. All of the samples are very fine-grained yellow powders, which were washed in de-ionized water, filtered, and air dried prior to X-ray analysis.

Data were collected and unit-cell parameters were determined for several of the natural samples. Dry, ground samples were sieved through a 210 μm mesh on to a zero-background silicon plate to reduce preferred orientation. The Topaz Academic software package was used to determine unit-cell parameters. Starting parameters were taken from Majzlan et al. (2004) and the unit-cell parameters were refined. Starting parameters from hydronium jarosite were chosen as unit-cell parameter *c* is approximately midway between jarosite and natrojarosite. Atomic coordinates and site occupancies were not refined.

The samples were analyzed using an Amray 1830 scanning electron microscope (SEM) and Link ISIS Oxford Systems energy-dispersive spectrometer (EDS). Results confirmed the presence or absence of elemental substitutions in the A or B sites, which aided in the interpretation of the unit-cell parameters.

Analyses of natural samples reported in the literature were reviewed and unit-cell parameters were plotted along with data from synthetic samples produced in this study. Chemical analyses were not available for the majority of the samples, so samples that were labeled as jarosite, hydronium jarosite, or natrojarosite that have unit-cell dimension $a < 7.29$ Å were not studied further as they most likely contained substantial Al substitution in the B site. Al in the B site causes a reduction in unit-cell parameter *a* (Brophy et al. 1962).

Results and discussion

Sample synthesis and homogeneity

It was found in the synthesis experiments that samples produced in the Na-H_3O jarosite solid-solution series differed in sample homogeneity through the series. Samples that had below 50% Na occupancy in the A site were homogeneous with no peak splitting (samples S, T, and U, where starting solutions contained 1.0, 0.6, and 0.2 g of Na_2SO_4). Starting solutions with above 1.0 g of Na_2SO_4 resulted in spectra with broadening of the 006 peak. Peak broadening is most evident for peak 006 where there is a large difference in peak position between Na-rich and Na-poor phases in the mixture (see Fig. 1 in Basciano and Peterson 2007). When annealed, these samples did become homogeneous with >85% Na occupancies when more than 1.0 g of Na_2SO_4 was used in the starting solution. To complete the solid-solution series, samples with 0.7 and 0.85 g of Na_2SO_4 in the starting solution produced samples with 68.6 and 87.5% Na occupancy in the final product after annealing. Samples below 50% Na occupancy in the final product did not require annealing as they were homogeneous. It was found that when samples with below 50% Na were annealed at 140 °C in the original solution the resulting jarosite product increased in Na content.

End-member natrojarosite with the A site fully occupied with Na could not be grown using the chloride method even though the other compositions in the $(Na)_{1-x}K_xFe_3(SO_4)_3(OH)_6$ solid-solution series could be grown. The resulting product when using the chloride method had ~90% Na occupancy. This may occur because natrojarosite and hydronium jarosite have similar solubilities (Glynn 2000). In systems where there is a large difference in the solubilities of end-members, the first phase to precipitate out of solution is the less soluble end-member component. In the jarosite-natrojarosite series, jarosite is the first to precipitate and dominates. In the natrojarosite-hydronium jarosite series, neither end-member is dominant. End-member solubility products from PHREEQC (Parkhurst and Appelo 2000) are $10^{-5.28}$ for natrojarosite, $10^{-5.39}$ for hydronium jarosite, and $10^{-9.21}$ for jarosite.

As in the K-H_3O jarosite solid-solution series (Basciano and Peterson 2007), K-rich jarosite precipitated out of solution first in the Na-K series, followed by Na-rich jarosite. During initial X-ray scans the 006 peak was often split indicating two jarosite phases with intermediate compositions between Na and K jarosite. After annealing at 140 °C for up to 6 days the samples became homogeneous, as determined by peak widths. From these experiments it was found that a single phase is stable at 140 °C for any composition in the K-H_3O and K-Na series.

The zoning seen in the synthetic samples is common in nature. Oscillatory zoning was found by Papike et al. (2007) in several natural samples. The zoning is probably caused by a similar mechanism as in the current experiments, where K in the solution is taken up in the jarosite structure before Na. The variation in the composition of natural samples discussed by Papike et al. (2007) probably reflects a change in fluid composition during crystallization.

Solid solution and structural parameters

Synthetic samples. There is a progressive change in unit-cell parameters for both solid-solution series $(Na)_{1-x}(H_3O)_x$ $Fe3(SO_4)_3(OH)_6$ and $(Na)_{1-x}K_xFe_3(SO_4)_3(OH)_6$ with increasing Na content. From chemical analysis and unit-cell dimensions determined by Rietveld refinement, all samples have full Fe occupancy and the A site in the $(Na)_{1-x}K_xFe_3(SO_4)_3(OH)_6$ solid-solution series is completely occupied by Na and/or K. The reliability factors, positional parameters, site occupancies, and selected interatomic distances and angles obtained are given in Tables 2, 3, and 4.

A structural drawing of natrojarosite is shown in Figure 2. The jarosite group crystallizes in space group $R\bar{3}m$, with $Z = 3$ (in the hexagonal unit cell). The basic structure of the jarosite group consists of SO_4 tetrahedra and Fe-cation octahedra, where the octahedra corner-share to form sheets perpendicular to the

TABLE 3. Refined atomic positions, displacement parameters, and occupancies of synthetic and natural jarosite samples

Site	W	x	y	z	B	Occ
Sample K						
Na	3*a*	0	0	0	0.7(1)	0.26
K	3*a*	0	0	0	0.7(1)	0.78
Fe	9*d*	0.166667	–0.166667	–0.16667	2.27(9)	1
S	6*c*	0	0	0.3091(2)	1.6(1)	1
O1	6*c*	0	0	0.3947(4)	2.4(3)	1
O2	18*h*	0.2226(3)	–0.2226(3)	–0.0542(3)	1.9(2)	1
O3	18*h*	0.1275(2)	–0.1275(2)	0.1325(2)	0.6(1)	1
H	18*h*	0.165(1)	–0.165(1)	0.168(2)	2	1
Sample L						
Na	3*a*	0	0	0	1.0(2)	0.41
K	3*a*	0	0	0	1.0(2)	0.61
Fe	9*d*	0.166667	–0.166667	–0.16667	2.6(1)	1
S	6*c*	0	0	0.3096(3)	1.5(1)	1
O1	6*c*	0	0	0.3952(5)	2.4(3)	1
O2	18*h*	0.2236(3)	–0.2236(3)	–0.0541(3)	2.2(2)	1
O3	18*h*	0.1275(3)	–0.1275(3)	0.1333(2)	0.3(1)	1
H	18*h*	0.161(1)	–0.161(1)	0.172(2)	2	1
Sample M						
Na	3*a*	0	0	0	1.9(2)	0.46
K	3*a*	0	0	0	1.9(2)	0.52
Fe	9*d*	0.166667	–0.166667	–0.16667	2.14(9)	1
S	6*c*	0	0	0.3102(3)	1.2(2)	1
O1	6*c*	0	0	0.3945(5)	2.0(3)	1
O2	18*h*	0.2246(3)	–0.2246(3)	–0.0540(3)	1.9(2)	1
O3	18*h*	0.1271(2)	–0.1271(2)	0.1325(2)	0.4(2)	1
H	18*h*	0.157(2)	–0.157(2)	0.173(2)	2	1
Sample N						
Na	3*a*	0	0	0	2.5(2)	0.69
K	3*a*	0	0	0	2.5(2)	0.29
Fe	9*d*	0.166667	–0.166667	–0.16667	2.02(7)	1
S	6*c*	0	0	0.3112(2)	0.7(1)	1
O1	6*c*	0	0	0.3972(4)	1.9(3)	1
O2	18*h*	0.2252(3)	–0.2252(3)	–0.0528(3)	1.1(2)	1
O3	18*h*	0.1267(2)	–0.1267(2)	0.1315(2)	0.2(2)	1
H	18*h*	0.162(2)	–0.162(2)	0.170(2)	2	1
Sample O						
Na	3*a*	0	0	0	3.4(2)	0.85
K	3*a*	0	0	0	3.4(2)	0.11
Fe	9*d*	0.166667	–0.166667	–0.16667	1.62(6)	1
S	6*c*	0	0	0.3121(2)	1.2(1)	1
O1	6*c*	0	0	0.4008(3)	1.4(2)	1
O2	18*h*	0.2229(2)	–0.2229(2)	–0.0510(2)	1.5(1)	1
O3	18*h*	0.1257(1)	–0.1257(1)	0.1305(1)	0.4(1)	1
H	18*h*	0.162(1)	–0.162*1)	0.169	2	1
Sample P						
Na	3*a*	0	0	0	3.0(1)	1.0
K	3*a*	0	0	0	3.0(1)	0.0
Fe	9*d*	0.166667	–0.166667	–0.16667	1.09(4)	1
S	6*c*	0	0	0.3123(1)	0.91(6)	1
O1	6*c*	0	0	0.4020(2)	0.8(1)	1
O2	18*h*	0.2220(2)	–0.2220(2)	–0.0505(1)	0.85(8)	1
O3	18*h*	0.1252(1)	–0.1252(1)	0.13018(9)	0.33(8)	1
H	18*h*	0.1583(9)	–0.1583(9)	0.1697(9)	2	1
Sample Q						
Na	3*a*	0	0	0	3.0(1)	0.87
H_3O	3*a*	0	0	0	3.0(1)	0.13
Fe	9*d*	0.166667	–0.166667	–0.16667	1.43(5)	1
S	6*c*	0	0	0.3117(1)	1.16(9)	1
O1	6*c*	0	0	0.4012(2)	1.0(2)	1
O2	18*h*	0.2222(2)	–0.2222(2)	–0.0510(1)	1.3(1)	1
O3	18*h*	0.1252(1)	–0.1252(1)	0.1304(1)	0.64(9)	1
H	18*h*	0.1671(9)	–0.1671(9)	0.164(1)	2	1
Sample R						
Na	3*a*	0	0	0	3.5(2)	0.67
H_3O	3*a*	0	0	0	3.5(2)	0.33
Fe	9*d*	0.166667	–0.166667	–0.16667	1.70(5)	1
S	6*c*	0	0	0.3111(1)	0.99(9)	1
O1	6*c*	0	0	0.3995(3)	1.0(2)	1
O2	18*h*	0.2235(3)	–0.2235(3)	–0.0522(2)	1.4(1)	1
O3	18*h*	0.1255(1)	–0.1255(1)	0.1308(1)	0.68(9)	1
H	18*h*	0.166(1)	–0.166(1)	0.166(1)	2	1
Sample S						
Na	3*a*	0	0	0	5.4(2)	0.49
H_3O	3*a*	0	0	0	5.4(2)	0.51
Fe	9*d*	0.166667	–0.166667	–0.16667	1.66(4)	1
S	6*c*	0	0	0.3099(1)	1.44(7)	1
O1	6*c*	0	0	0.3990(3)	1.4(2)	1
O2	18*h*	0.2235(2)	–0.2235(2))	–0.0535(2)	1.9(1)	1
O3	18*h*	0.1255(1)	–0.1255(1)	0.1320(1)	0.42(9)	1
H	18*h*	0.166(1)	–0.166(1)	0.166(1)	2	1
Sample T						
Na	3*a*	0	0	0	8.0(3)	0.35
H_3O	3*a*	0	0	0	8.0(3)	0.65
Fe	9*d*	0.166667	–0.166667	–0.16667	1.84(5)	1
S	6*c*	0	0	0.3089(2)	1.81(9)	1
O1	6*c*	0	0	0.3979(3)	0.5(2)	1
O2	18*h*	0.2229(2)	–0.2229(2)	–0.0538(2)	2.6(1)	1
O3	18*h*	0.1257(1)	–0.1257(1)	0.1326(2)	0.5(1)	1
H	18*h*	0.171(1)	–0.171(1)	0.163(1)	2	1
Sample U						
Na	3*a*	0	0	0	7.1(3)	0.24
H_3O	3*a*	0	0	0	7.1(3)	0.76
Fe	9*d*	0.166667	–0.166667	–0.16667	2.11(6)	1
S	6*c*	0	0	0.3094(2)	1.9(1)	1
O1	6*c*	0	0	0.3998(3)	2.2(2)	1
O2	18*h*	0.2242(2)	–0.2242(2)	–0.0548(2)	2.8(1)	1
O3	18*h*	0.1266(1)	–0.1266(1)	0.1338(1)	0.3(1)	1
H	18*h*	0.169(1)	–0.169(1)	0.167(1)	2	1

Note: Numbers in parentheses in this and subsequent tables are estimated standard deviations, A site occupancies determined with ICP-OES.

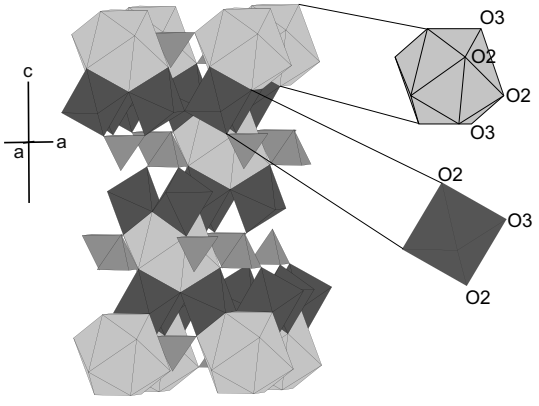

FIGURE 2. Polyhedral representation of the natrojarosite structure. Sodium polyhedra (A site) are light gray, Fe octahedra are dark gray (B site), and sulfate tetrahedra are medium gray.

c axis. The SO_4 tetrahedra have two orientations within a layer; one set of tetrahedra points toward +*c* and alternates with another set pointing toward –*c*. Twelve anions, consisting of six oxygen atoms (O2) and six OH groups (O3) form an icosahedron, in which the alkali cation (K^+, H_3O^+, Na^+, etc.) is located.

Natrojarosite has a much smaller unit-cell volume than K jarosite and hydronium jarosite as a result of the smaller diameter of Na^+, 1.39 Å, than K^+, 1.64 Å and H_3O^+, 1.52 Å (Shannon 1976; Dutrizac and Jambor 2000). Substitution of Na into K jarosite decreases unit-cell parameter *c* significantly (0.617 Å) and increases *a* to a minor degree (0.012 Å). Substitution of Na into hydronium jarosite decreases unit-cell parameter *c* significantly (0.408 Å) and decreases *a* (0.040 Å).

The unit-cell parameters *a* vs. *c* for solid-solution series $(Na)_{1-x}(H_3O)_xFe_3$-$(SO_4)_3(OH)_6$ and $(Na)_{1-x}K_xFe_3(SO_4)_3(OH)_6$ from the current study and solid-solution series $(K)_{1-x}(H_3O)_x$ $Fe_3(SO_4)_3(OH)_6$ from Basciano and Peterson (2007) are plotted

TABLE 4. Selected interatomic distances (Å) and angles (°)

A site	I*	K	L	M	N	O	P	Q	R	S	T	U	A*
occ (%)	H_3O 5 K 95	Na 26 K 78	Na 41 K 61	Na 46 K 52	Na 69 K 29	Na 85 K 11	Na 100 K 0	Na 87 H_3O 13	Na 67 H_3O 33	Na 49 H_3O 51	Na 35 H_3O 65	Na 24 H_3O 76	H_3O 100
K,Na-O3 × 6	2.802(2)	2.780(3)	2.778(3)	2.757(3)	2.727(3)	2.694(2)	2.679(1)	2.689(2)	2.706(2)	2.734(2)	2.748(2)	2.780(2)	2.839(2)
K,Na-O2 × 6	2.949(2)	2.965(4)	2.974(4)	2.985(5)	2.986(4)	2.949(3)	2.935(2)	2.942(2)	2.968(3)	2.980(2)	2.976(2)	3.000(3)	3.026(4)
Average	2.876	2.873	2.876	2.871	2.857	2.822	2.807	2.816	2.837	2.857	2.862	2.890	2.933
Fe-O3 × 4	1.9806(7)	1.997(1)	1.992(1)	1.995(1)	1.997(1)	1.9983(8)	1.9980(2)	1.9985(7)	1.9999(3)	1.9982(7)	1.9971(8)	1.9963(8)	1.9904(9)
Fe-O2 × 2	2.050(2)	2.048(4)	2.042(5)	2.040(6)	2.049(4)	2.053(2)	2.050(2)	2.049(3)	2.045(3)	2.035(2)	2.032(3)	2.030(3)	2.015(4)
Average	2.015	2.023	2.017	2.018	2.023	2.026	2.024	2.024	2.022	2.017	2.015	2.013	2.003
S-O1	1.463(5)	1.462(8)	1.454(8)	1.425(2)	1.441(7)	1.477(6)	1.489(4)	1.489(4)	1.478(4)	1.498(5)	1.489(3)	1.484(3)	1.447(7)
S-O2 × 3	1.510(2)	1.491(4)	1.481(4)	1.473(5)	1.462(4)	1.484(3)	1.492(2)	1.492(3)	1.480(2)	1.485(2)	1.502(4)	1.531(6)	1.485(4)
Average	1.487	1.477	1.468	1.449	1.452	1.481	1.491	1.491	1.479	1.492	1.496	1.508	1.466
O2-Fe-O3 × 4	87.65(7)	87.2 (1)	88.0(1)	88.0(1)	87.9(1)	86.93(8)	86.63(6)	86.75 (5)	87.25(7)	87.84(7)	87.90(7)	88.75(7)	89.6(1)
O2-Fe-O3 × 4	92.35(7)	92.8 (1)	92.0(1)	92.0 (1)	92.2(1)	93.07 (8)	93.37 (6)	93.25(5)	92.75(7)	92.16(7)	92.10(7)	91.25(7)	90.4(1)
O3-Fe-O3 × 2	87.67(8)	88.8(1)	89.1(1)	88.6(2)	88.2(1)	87.3(1)	86.87(8)	86.89(8)	87.20(9)	87.52(9)	87.73(9)	88.6(1)	89.7(1)
O3-Fe-O3 × 2	92.33(8)	91.2 (1)	90.9 (1)	91.4(2)	91.9(1)	92.7(1)	93.13(8)	93.11(8)	92.80(9)	92.48(9)	92.27(9)	91.4(1)	90.3(1)
O1-S-O2 × 3	109.93(8)	110.1(2)	110.3(2)	110.8(2)	110.5(2)	109.5(1)	109.10(6)	109.2(1)	109.8(1)	109.9(1)	109.4(1)	110.6(2)	112.0(1)
O2-S-O2 × 3	109.01(8)	108.8(2)	108.6(2)	108.1(3)	108.3(2)	109.4(2)	109.8(1)	109.7(1)	109.2(1)	109.0(1)	109.5(1)	108.3(2)	106.9(2)
Average	109.5	109.5	109.5	109.5	109.4	109.5	109.5	109.5	109.5	109.5	109.5	109.5	109.5
O3-H	0.779(1)	0.77(3)	0.78(3)	0.79(3)	0.78(3)	0.79(2)	0.78(2)	0.78(2)	0.775(2)	0.77(2)	0.775(2)	0.775(2)	0.767(2)
O3-H ··· O1	2.923(2)	2.874(4)	2.872(3)	2.875(4)	2.852(3)	2.833(2)	2.828(1)	2.837(1)	2.850(2)	2.867(2)	2.880(2)	2.868(3)	2.914(3)

* From Basciano and Peterson (2007).

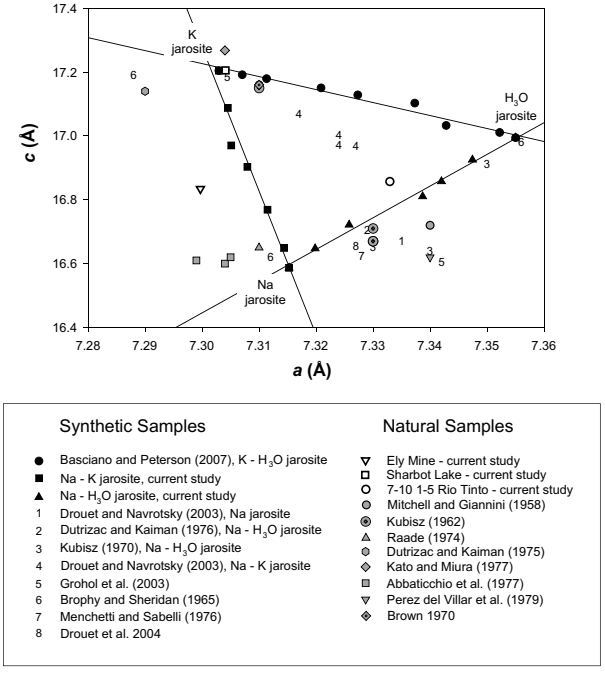

FIGURE 3. Unit-cell parameters *a* vs. *c* of synthetic Na-H_3O and Na-K jarosite series from the current study, synthetic samples from previous studies that contain Na, K, and H_3O or Na and H_3O in the A site and natural jarosite samples that contain varying amounts of Na, K, and H_3O. All samples from the current synthetic study are shown as black squares or triangles. Note that the unit-cell dimensions fall close to a straight line, and unit-cell parameter *c* is larger than most of the previous synthetic studies as the B site is fully occupied. Data from previous synthetic studies are shown as numbers and natural samples are shown as gray symbols. Samples labeled 4 contain Na and K in the A site and have Fe deficiencies in the B site causing a shift down and to the right of the Na-K solid solution line. Samples below the Na-H_3O solid solution line have Fe deficiencies in the B site causing a reduction in unit-cell parameter *c*.

in Figure 3. Data from previous studies of Na-hydronium jarosite and Na-K jarosite solid-solution series are also included on the plot. For clarity, data from previous synthetic studies of the K-H_3O jarosite solid-solution series, other than those from Basciano and Peterson (2007), are not included . The majority of synthetic K-H_3O samples plot below those from Basciano and Peterson (2007) due to Fe deficiency. The data from this study fall close to straight lines for both the Na-hydronium jarosite series (coefficient of determination $r^2 = 0.99$) and the Na-K jarosite series ($r^2 = 0.97$), following Vegard's law of ideal solid solution. Variation of the unit-cell parameters vs. Na content for the Na-hydronium jarosite series and Na-K series are presented in Figure 4.

It was found by Basciano and Peterson (2007) that an Fe deficiency in the B site causes a significant reduction in unit-cell parameter *c*. The majority of synthetic jarosite group minerals grown in previous studies do have Fe deficiencies in the B site, causing a reduction in *c*. As a result of full Fe occupancy in the synthetic samples grown in the current study, *c* cell dimensions of the Na-H_3O and Na-K jarosite solid-solution series are larger than most previous work with comparable A site occupancies. Additionally, there is no substitution in the A site by H_3O^+ in our Na-K jarosite series. Well-defined trends can be seen in the unit-cell parameters across the solid-solution series in the synthetic samples from this study and Basciano and Peterson (2007).

End-member K jarosite with full Fe occupancy was grown by Grohol et al. (2003) (labeled 5 in Fig. 3) and the unit-cell parameters closely match end-member K jarosite reported in Basciano and Peterson (2007). Natrojarosite grown by Grohol et al. (2003) was reported to be stoichiometric with respect to Fe and with full Na occupancy, but the unit-cell parameters are not similar to the natrojarosite grown in this study and do not follow the trend of the solid-solution series. Unit-cell parameter *c* is similar for both samples but *a* is significantly larger than for the sample grown in this study. The unit-cell parameters for natrojarosite grown by Grohol et al. (2003) are similar to a sample grown by Kubisz (1970), which has a formula of

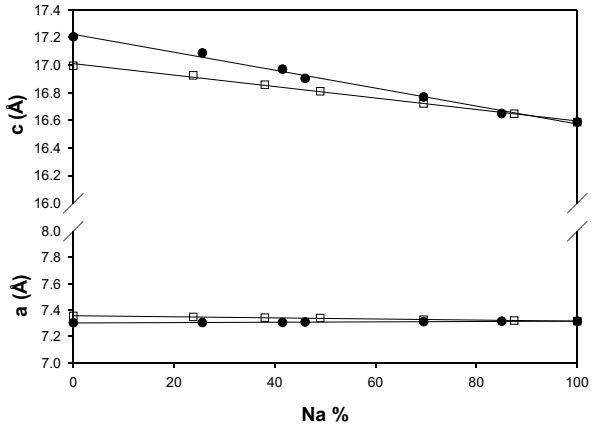

FIGURE 4. Unit-cell dimensions *a* and *c* vs. Na occupancy in the A site for synthetic samples in this study. Black circles represent samples from the Na-K series and white squares represent samples from the Na-H_3O series. Error bars reported by Rietveld refinement are smaller than the symbols.

$Na_{0.67}(H_3O)_{0.33}Fe_{2.83}(SO_4)_2(OH)_{5.49}(H_2O)_{0.51}$.

Previous samples grown in the Na-K jarosite solid-solution series by Drouet and Navrotsky (2003) (labeled 4 on Fig. 3) contain ~30% H_3O in the A site and are Fe deficient by 11–14% in the B site. Hydronium substitution causes a unit-cell parameter shift toward end-member hydronium jarosite and the Fe deficiency causes a decrease in unit-cell parameter *c*. In Figure 3, the Drouet and Navrotsky (2003) samples plot to the right of the K-Na jarosite samples synthesized in this study as they are a solid solution between jarosite, natrojarosite, and hydronium jarosite. The samples do not have a uniform level of Fe deficiency; Fe occupancy of the samples ranges from 2.57 to 2.67. If the samples had full Fe occupancy, they should plot on tie lines from the Na-K solid solution line to hydronium jarosite. As there is a difference in the Fe occupancy of the samples, there is considerable scatter, and correlation between Na and K content in the A site and unit-cell parameters is lost as unit-cell parameter *c* is affected by both A site content and Fe deficiency in the B site. Samples from previous studies in the Na-H_3O jarosite solid-solution series that are Fe deficient (Kubisz 1970; Dutrizac and Kaiman 1976; Drouet and Navrotsky 2003) plot below the samples grown in this study in Figure 3.

Polyhedral bond lengths A-O2 and A-O3 and Fe-O2 and Fe-O3 for Na-H_3O jarosite, Na-K jarosite and K-H_3O (Basciano and Peterson 2007) solid-solution series are shown in Figure 5. Data were included for the K-H_3O jarosite solid-solution series for completeness. Polyhedral bond lengths of the A and B site vary linearly with occupancy. With Na substitution into K jarosite, A-O3 decreases and A-O2 decreases to a very minor degree. Correspondingly, Fe-O3 increases and Fe-O2 increases to a minor degree.

Similarly in the Na-H_3O jarosite solid-solution series, bond lengths A-O3 and A-O2 decrease with Na substitution, and Fe-O3 and Fe-O2 increase. As proposed in Basciano and Peterson (2007), it is assumed that the hydrogens of the H_3O groups are hydrogen bonded to the O2 atoms in the A polyhedra, based on hydronium geometry. The A-O3 bond length is affected more significantly in the Na-H_3O series than in K-H_3O series. This is likely caused by the much smaller ionic radius of Na^+ than H_3O^+. Both A-O2 and A-O3 decrease by a similar degree (0.09 and 0.16 Å, respectively), while Fe-O2 increases by 0.035 Å, and Fe-O3 increases by only 0.0076 Å. A similar trend is seen in the Na-K solid-solution series for the Fe polyhedra. As the A polyhedra are face sharing with the Fe octahedra and O3 is a hydroxyl group that is hydrogen bonded to O1 of the sulfate group, there is less possible flexibility in the Fe-O3 bond length. Substitutions in the A site mainly effect the Fe-O2 bond length. As determined by the differences in maximum and minimum bond lengths, the A polyhedra in the Na-H_3O series remain distorted as Na content increases, while the Fe octahedra become increasingly distorted as Na increases. In the Na-K series, the A polyhedra become increasingly distorted as Na increases and the distortion of the Fe octahedra remains relatively constant across the series.

Natural samples. Unit-cell parameters of three natural samples were measured in this study and are plotted in Figure 3. The Sharbot Lake sample appears to be a stoichiometric K jarosite and has very similar unit-cell parameters to synthetic stoichiometric K jarosite, with unit-cell parameters *a* 7.304(1), *c* 17.206(4) Å. No Al or Na was found during EDS analysis. The sample analyzed from Ely Mine, Vermont contains both Na and K in roughly similar proportions. The sample plots approximately halfway between Na jarosite and K jarosite, to the left of the synthetic samples. The *a* parameter is ~0.01 Å less than the synthetic samples. These results suggest that there is a minor amount of Al in the sample as this would cause a reduction in the *a* parameter. The presence of Al was confirmed with SEM-EDS analysis. Sample 7-10 1-5 from Rio Tinto, Spain has unit-cell parameters *a* 7.333(2) and *c* 16.856(4) Å, and plots approximately halfway between hydronium jarosite and natrojarosite. The sample plots above the synthetic samples indicating that either there is K substituting into the A site or Al substituting into the B site. SEM-EDS analysis indicates a minor amount of Al in the sample and no K. Al substitution would cause a decrease in unit-cell parameter *a* and no change in *c* (Brophy et al. 1962). Potassium substitution would have caused a decrease in unit-cell parameter *a* and an increase in *c*.

Unit-cell parameters from natural samples reported in the literature were also plotted on Figure 3. No chemical analyses were reported for the majority of the samples. The samples that plot to the left of the synthetic K-Na jarosite samples probably have Al substitution in the B site, causing a reduction in unit-cell parameter *a*. Three of the samples analyzed by Abbaticchio et al. (1977) do have minor amounts of Al, which causes the small reduction in *a* relative to our synthetic samples. In Figure 3, it can be seen that several of the natural specimens plot close to the synthetic samples grown in this study and by Basciano and Peterson (2007), indicating near to full Fe occupancy in the B site. From these results and natural samples analyzed in Basciano and Peterson (2007) and Papike et al.(2007), it is probable that many natural jarosite samples have close to full occupancy of the B site. The jarosite group members synthesized in this study are probably more similar to many natural samples than jarosites synthesized in earlier studies, which likely have Fe-deficiencies.

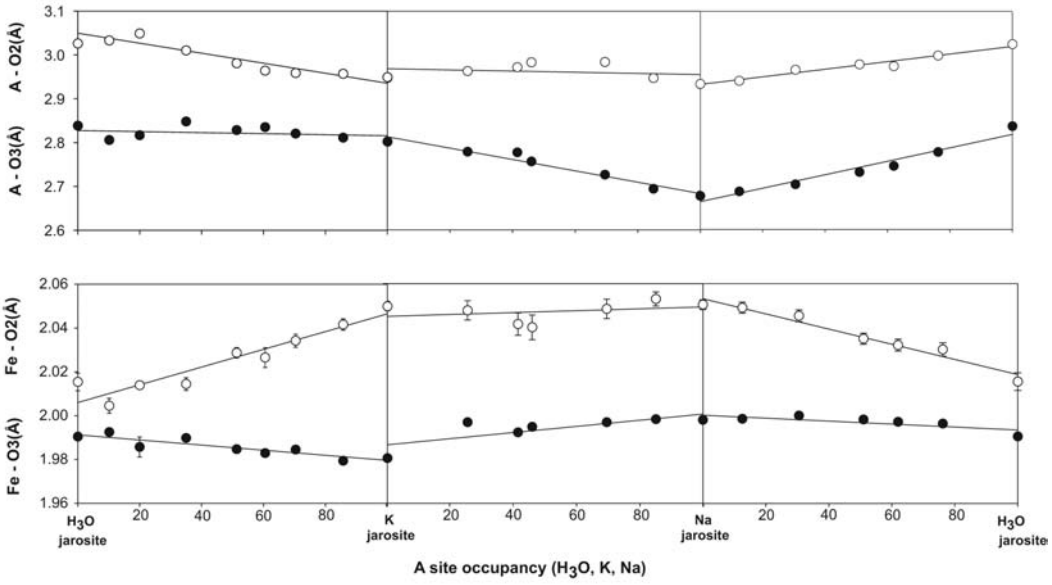

FIGURE 5. A-O polyhedra bond lengths and Fe-O octahedral bond lengths vs. A site occupancy in the Na-H_3O, Na-K, and K-H_3O series. Data from the K-H_3O jarosite solid-solution series is taken from Basciano and Peterson (2007).

Hydronium in the jarosite group

The presence of hydronium in jarosite and alunite has been investigated in several studies. The most recent study done by Nielson et al. (2007) found that H_3O^+ is not found in alunite or natroalunite in solid state NMR studies that have both A and B site deficiencies. They did see evidence for H_3O^+ in hydronium alunite. Nielson et al. (2007) postulated that vacancies in the B site are compensated by the addition of 4 H^+ ions, resulting in 4 Al-OH_2 bonds per vacancy. This substitution is accompanied by deprotonation of H_3O^+ in the A site, forming H_2O, which is then unnecessary for charge balance resulting in an A site vacancy. As the complete solid-solution series between K-H_3O jarosite and Na-H_3O jarosite in this study and Basciano and Peterson (2007) have been synthesized with no B site vacancies, it is probable that hydronium exists through the series in the A site. In samples that contain B site vacancies, it is possible that an addition of H^+, creating 4 Fe-OH_2 groups per B site vacancy and subsequent vacancy in the A site would occur for only several the A sites. As all of the B site vacancies are compensated there would be no additional vacancies created in the A site, the remaining A sites are likely filled with H_3O^+. It is common to see as much as 13% vacancy in the B site of jarosite in synthetic studies, and it is probable that a similar percentage of A sites are vacant and the remaining occupancy of the A site that is not Na^+ or K^+ is H_3O^+.

SWIR and MIR

Short-wave infrared (SWIR) reflectance spectra and infrared (IR) spectra are shown in Figures 6 and 7. SWIR region data were collected for both the Na-H_3O and Na-K jarosite solid-solution series. The SWIR data for the Na-H_3O jarosite solid-solution series is shown in entirety, including the spectrum for hydronium jarosite taken from Basciano and Peterson (2007), for completeness. Only one spectrum from the Na-K solid-solution series is shown in Figure 6 as the differences in band shape and position in the spectra are subtle. The spectra are typical of the jarosite structure and the vibrational features have been labeled with assignments from Bishop and Murad (2005). In the Na-H_3O jarosite solid-solution series, there is a change in spectra that can be tracked across the series. Similar to the SWIR spectra for the K-H_3O jarosite solid-solution series analyzed in Basciano and Peterson (2007), detail is lost from the spectra across the series with increasing hydronium content. Bands that are dampened or lost are shoulders at 1514, 2214, 2296 nm, and the area between 2380 and 2500 nm. Detailed assignments of the bands are given in Figure 7.

Mid-infrared absorbance data were collected for samples in the K-H_3O, Na-H_3O, and Na-K jarosite solid-solution series. Samples in the K-H_3O series are from the previous study of Basciano and Peterson (2007). For clarity, only spectra for end-members and two samples within each series are included in Figure 7. Infrared spectra for jarosite group members have been reported and discussed elsewhere as well (Kubisz 1972; Powers et al. 1975; Baron and Palmer 1996; Drouet and Navrotsky 2003; Drouet et al. 2004; Bishop and Murad 2005; Frost et al. 2006). The absorbance spectra shown here are similar to those presented in the literature. What can be seen in these spectra is the change that occurs across the solid-solution series, especially changes due to the effect of H_3O. Spectral detail is lost with substitution of H_3O when H_3O transfers a proton to make OH_2. The OH_2 disrupts vibrational coupling causing some absorption features to disappear (Swayze et al. 2006). As many of the samples synthesized in this study have little to no H_3O the differences are apparent in the spectra. Band assignments for vibrational features are given in Table 5. There is some evidence of minor H_3O in the K jarosite spectrum, which was expected as the K jarosite analyzed has 95% K and 5% H_3O occupancy in the A site. There is no evidence for H_3O in the Na jarosite spectrum. There are minor changes between the Na and K jarosite spectra with

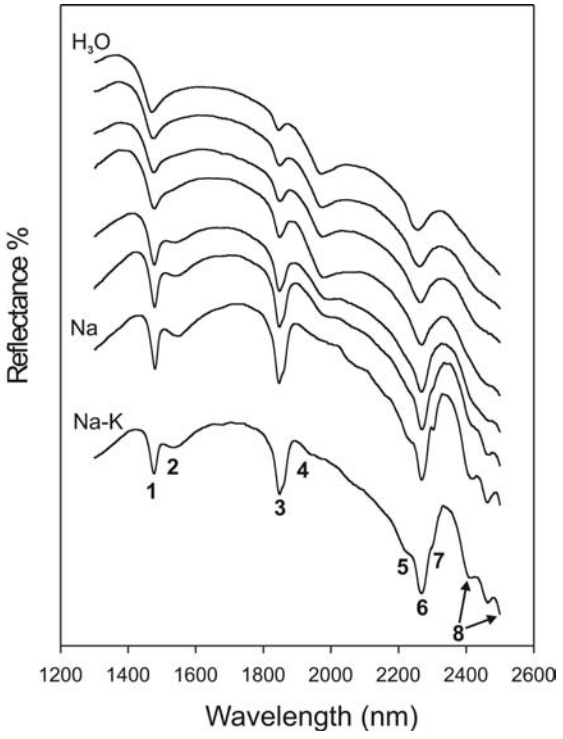

FIGURE 6. Short-wave infrared reflectance spectra of samples from the Na-H_3O jarosite solid-solution series and sample M from the Na-K jarosite solid-solution series. The bands have been assigned to the following: 1 = OH vibrations; 1,2 = OH stretch overtones; 3 = OH stretch and Fe-OH bend; 4 = H_2O and H_3O combination band absorption; 5, 6, 7 = Fe-OH combination bands (out of plane) and Fe-OH combination bands (in plane); and 8 = $(SO_4)_2$ stretching and OH vibration. Band assignments are from Bishop and Murad (2005) and Swayze (written comm.). Spectra have been offset vertically for comparison.

TABLE 5. Band assignments for vibrational features in synthetic K, H_3O, and Na jarosite

K jarosite	H_3O jarosite	Na jarosite	Assignment
445	464 b	445	$\nu_2(SO_4)^{2-}$
466	–	474	Fe-O
503	503	503	Fe-O
577 sh	–	584 sh	γ(OH)
627	623	627	$\nu_4(SO_4)^{2-}$
665	–	682	$\nu_4(SO_4)^{2-}$
999	1004	1006	δ(OH)
~1022 sh	–	~1014 sh	δ(OH)
1083	1089	1091	$\nu_3(SO_4)^{2-}$
1184	1195	1172	$\nu_3(SO_4)^{2-}$
–	1576 sh	–	$\delta(H_2O)$
1639 vw	1639	–	$\delta(H_2O)$
3384	3367 b	3353	ν(OH)

Notes: sh = shoulder, b = wide, vw = very weak. Band assignments are from Bishop and Murad (2005).

minor peak shifts as a result of the difference in energies caused by the degree of interpenetration controlled by A site cation size (Drouet and Navrotsky 2003). Hydronium in the A site causes peak shifts as well as peak widening (464 cm^{-1}) or elimination of peaks (466, 577 shoulder, and 665 cm^{-1} in K jarosite). H_3O jarosite does have one peak and shoulder missing or very weak in both K jarosite and Na jarosite (1639 and 1576 cm^{-1}) that are assigned to the water band (δH_2O).

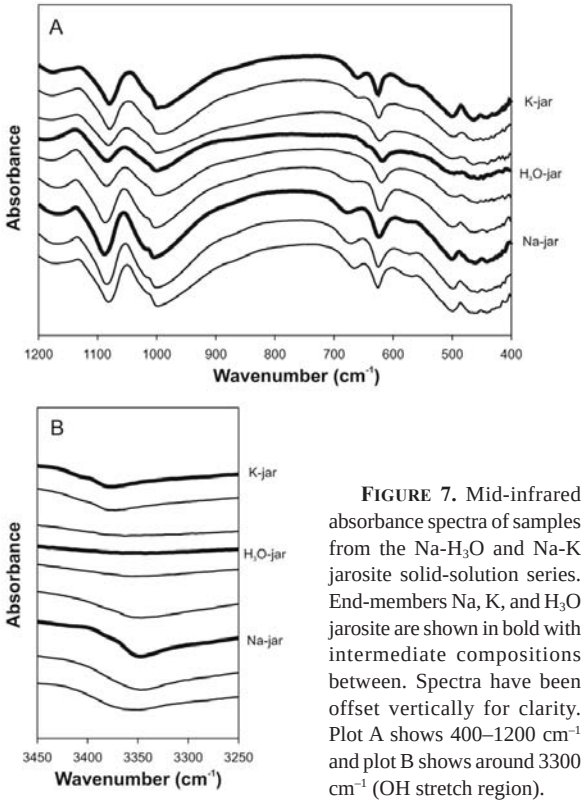

FIGURE 7. Mid-infrared absorbance spectra of samples from the Na-H_3O and Na-K jarosite solid-solution series. End-members Na, K, and H_3O jarosite are shown in bold with intermediate compositions between. Spectra have been offset vertically for clarity. Plot A shows 400–1200 cm^{-1} and plot B shows around 3300 cm^{-1} (OH stretch region).

CONCLUDING REMARKS

Data provided in this study as well as other recent advances in knowledge of the jarosite group of minerals (Glynn 2000; Papike et al. 2007; Nielson et al. 2007) will aid in the interpretation of jarosite group minerals analyzed in future Mars missions where the combined XRD/XRF (CheMin) instrument will be used. For such an instrument to be successful at discriminating different jarosite compositions, it must have a resolution sufficient to employ Figure 3 in this study. As discussed in Papike et al. (2007), the X-ray patterns of martian jarosite may show two patterns, and the unit-cell analyses done in this study and by Basciano and Peterson (2007) will help in the interpretation of the possible chemical compositions of jarosite species encountered.

ACKNOWLEDGMENTS

The authors thank Queen's University Analytical Services for the chemical analysis of the samples. The research was funded by an NSERC discovery grant to R.C.P. We thank Gregg Swazye, an anonymous reviewer, and editor George Lager for their valuable comments on the manuscript.

REFERENCES CITED

Abbaticchio, P., Amicarelli, V., Balenzano, F., Di Pierro, M., Guerricchio, A., and Melidoro, G. (1977) Presence of natrojarosite in the variegated clays of Casignana and Plati (Reggio Calabria province) (Italy). Geologia Applicata e Idrogeologia, 12, 387–398.

Balzar, D. (1999) Voigt-function model in diffraction line-broadening analysis. International Union of Crystallography Monographs on Crystallography, 10, 94–126.

Baron, D. and Palmer, C.D. (1996) Solubility of jarosite at 4–35 ºC. Geochimica et Cosmochimica Acta, 60, 185–195.

Bartlett, B.M. and Nocera, D.G. (2005) Long-range magnetic ordering in Fe

jarosites prepared by redox-based hydrothermal methods. Journal of the American Chemical Society, 127, 8985–8993.
Basciano, L.C. and Peterson, R.C. (2007) Jarosite-hydronium jarosite solid-solution series with full Fe occupancy: Mineralogy and crystal chemistry. American Mineralogist, 92, 1464–1473.
Baur, W.H. (1972) Prediction of hydrogen bonds and hydrogen atom positions in crystalline solids. Acta Crystallographica, B28, 1456–1465.
Bishop, J.L. and Murad, E. (2005) The visible and infrared spectral properties of jarosite and alunite. American Mineralogist, 90, 1100–1107.
Brophy, G.P. and Sheridan, M.F. (1965) Sulfate studies IV: The jarosite-natrojarosite-hydronium jarosite solid solution series. American Mineralogist, 50, 1595–1607.
Brophy, G.P., Scott, E.S., and Snellgrove, R.A. (1962) Sulfate studies II: Solid solution between alunite and jarosite. American Mineralogist, 22, 773–784.
Brown, J.B. (1970) A chemical study of some synthetic K-hydronium jarosites. Canadian Mineralogist, 10, 696–703.
Cheary, R.W. and Coelho, A.A. (1998) Axial divergence in a conventional X-ray powder diffractometer I. Theoretical foundations. Journal of Applied Crystallography, 31, 851–861.
Coelho, A.A. (2004) TOPAS-Academic. http://members.optusnet.com.au/~alancoelho.
Drouet, C. and Navrotsky, A. (2003) Synthesis, characterization, and thermochemistry of K-Na-H_3O jarosites. Geochimica et Cosmochimica Acta, 11, 2063–2076.
Drouet, C., Pass, K.L., Baron, D., Draucker, S., and Navrotsky, A. (2004) Thermochemistry of jarosite-alunite and natrojarosite-natroalunite solid solutions. Geochimica et Cosmochimica Acta, 68, 2197–2205.
Dutrizac, J.E. (1983) Factors affecting alkali jarosite precipitation. Metallurgical Transactions, 14B, 531–539.
Dutrizac, J.E. and Jambor, J.L. (2000) Jarosites and their application in hydrometallurgy. In C.N. Alpers, J.L. Jambor and D.K. Nordstrom, Eds., Sulfate Minerals—Crystallography, Geochemistry, and Environmental Significance, 40, p. 405–452. Reviews in Mineralogy and Geochemistry, Mineralogical Society of America, Chantilly, Virginia.
Dutrizac, J.E. and Kaiman, S. (1976) Synthesis and properties of jarosite-type compounds. Canadian Mineralogist, 14, 151–158.
Frost, R.L., Wills, R., Matt, M.L., Musumeci, A.W., and Martens, W. (2005) Thermal decomposition of natural and synthetic plumbojarosites: Importance in "archeochemistry." Thermochimica Acta, 432, 30–35.
Frost, R.L., Wills, R., Klopprogge, J.T., and Martens, W.N. (2006) Thermal decomposition of hydronium jarosite $(H_3O)Fe_3(SO_4)_2(OH)_6$. Journal of Thermal Analysis and Calorimetry, 83, 213–218.
Glynn, P. (2000) Solid-solution solubilities and thermodynamics: Sulfates, carbonates, and halides. In C.N. Alpers, J.L. Jambor and D.K. Nordstrom, Eds., Sulfate Minerals—Crystallography, Geochemistry, and Environmental Significance, 40, p. 481–511. Reviews in Mineralogy and Geochemistry, Mineralogical Society of America, Chantilly, Virginia.
Greedan, J.E. (2001) Geometrically frustrated magnetic materials. Journal of Materials Chemistry, 11, 37–53.
Grohol, D. and Nocera, D.G. (2002) Hydrothermal oxidation-reduction methods for the preparation of pure and single crystalline alunites: Synthesis and characterization of a new series of vanadium jarosites. Journal of the American Chemical Society, 124, 2640–2646.
Grohol, D., Nocera, D.G., and Papoutsakis, D. (2003) Magnetism of pure Fe jarosites. Physical Review B: Condensed Matter and Materials Physics, 67, 064401/1–064401/13.
Harrison, A. (2004) First catch your hare*: the design and synthesis of frustrated magnet. Journal of Physics—Condensed Matter, 16, S553–S572.
Hendricks, S.B. (1937) The crystal structure of alunite and the jarosites. American Mineralogist, 22, 773–784.
Hill, R.J. and Flack, H.D. (1987) The use of the Durbin-Watson *d* statistic in Rietveld analysis. Journal of Applied Crystallography, 20, 356–361.
Hölzer, G., Fritsch, M., Deutsch, M., Härtwig, J., and Förster, E. (1997) $K\alpha_{1,2}$ and $K\beta_{1,3}$ X-ray emission lines of the 3^d transition metals. Physical Review A, 56, 4554–4568.
Hudson-Edwards, K.A., Schell, C., and Macklin, M.G. (1999) Mineralogy and geochemistry of alluvium contaminated by metal mining in the Rio Tinto area, southwest Spain. Applied Geochemistry, 14, 1015–1030.
Klingelhöfer, G., Morris, R.V., Bernhardt, B., Schroder, C., Rodionov, D., de Souza, P.A.J., Yen, A.S., Gellert, R., Evlanov, E.N., Zubkov, B., Foh, J., Bonnes, U., Kankeleit, E., Gutlich, P., Ming, D.W., Renz, F., Wdowiak, T.J., Squyres, S.W., and Arvidson, R.E. (2004) Jarosite and hematite at Meridiani Planum from Opportunity's Mössbauer spectrometer. Science, 306, 1740–1745.
Kubisz, J. (1970) Studies on synthetic alkali-hydronium jarosites. I. Synthesis of jarosite and natrojarosite. Mineralogia Polonica, 1, 47–57.
——— (1972) Studies on synthetic alkali-hydronium jarosite III. Infrared absorption study. Mineralogia Polonica, 3, 23–36.
Lager, G.A., Swayze, G.A., Loong, C.-H., Rotella, F.J., Richardson, J.W., and Stoffregan, R.E. (2001) Neutron spectroscopic study of synthetic alunite and oxonium-substituted alunite. Canadian Mineralogist, 39, 1131–1138.
Madden, M.E.E., Bodnar, R.J., and Rimstidt, J.D. (2004) Jarosite as an indicator of water-limited chemical weathering on Mars. Nature, 431(7010), 821–823.
Majzlan, J., Stevens, R., Boerio-Goates, J., Woodfield, B.F., Navrotsky, A., Burns, P.C., Crawford, M.K., and Amos, T.G. (2004) Thermodynamic properties, low-temperature heat-capacity anomalies, and single-crystal X-ray refinement of hydronium jarosite, $(H_3O)Fe_3(SO_4)_2(OH)_6$. Physics and Chemistry of Minerals, 31, 518–531.
Nielson, U.G., Majzlan, J., Phillips, B., Ziliox, M., and Grey, C.P. (2007) Characterization of defects and the local structure in natural and synthetic alunite $(K, Na, H_3O)Al_3(SO_4)_2(OH)_6$ by multi-nuclear solid-state NMR spectroscopy. American Mineralogist, 92, 587–597.
Nocera, D.G., Bartlett, B.M., Grohol, D., Papoutsakis, D., and Shores, M.P. (2004) Spin frustration in 2D kagomé lattices: A problem for inorganic synthetic chemistry. Chemistry—A European Journal, 10, 3851–3859.
Papike, J.J., Karner, J.M., and Shearer, C.K. (2006a) Comparitive planetary mineralogy: Implications of martian and terrestrial jarosite. A crystal chemical perspective. Geochimica et Cosmochimica Acta, 70, 1309–1321.
Papike, J.J., Karner, J.M., Spilde, M.N., and Shearer, C.K. (2006b) Terrestrial analogues of martian sulfates: Major and minor element systematics of alunite-jarosite from Goldfield, Nevada. American Mineralogist, 91, 1197–1200.
Papike, J.J., Burger, P.V., Karner, J.M., Shearer, C.K., and Lueth, V.W. (2007) Terrestrial analogues of martian jarosites: Major, minor element systematics and Na-K zoning in selected samples. American Mineralogist, 92, 444–447.
Parkhurst, D.L. and Appelo, C.A.J. (2000) User's guide to PHREEQC (Version 2)—A computer program for speciation, batch-reaction, one-dimensional transport, and inverse geochemical calculations. U.S. Geological Survey Water Resources Invest Report, 99–4259.
Powers, D.A., Rossman, G.R., Schugar, H.J., and Gray, H.B. (1975) Magnetic behavior and infrared spectra of jarosite, basic Fe sulfate and their chromate analogs. Journal of Solid State Chemistry, 13, 1–13.
Ripmeester, J.A., Ratcliff, C.I., Dutrizac, J.E., and Jambor, J.L. (1986) Hydronium ion in the alunite-jarosite group. Canadian Mineralogist, 24, 435–447.
Scott, K.M. (1987) Solid solution in, and classification of, gossan-derived members of the alunite-jarosite family, northwest Queensland, Australia. American Mineralogist, 72, 178–187.
Shannon, R.D. (1976) Revised effective ionic radii and systematic studies of interatomic distances in halides and chalcogenides. Acta Crystallographica, A32, 751–767.
Stoffregen, R.E. (1993) Stability relations of jarosite and natrojarosite at 150–250 °C. Geochimica et Cosmochimica Acta, 57, 2417–2429.
Stoffregen, R.E. and Alpers, C.N. (1987) Woodhouseite and svanbergite in hydrothermal ore deposits: Products of apatite destruction during advanced argillic alteration. Canadian Mineralogist, 25, 201–211.
Stoffregen, R.E., Alpers, C.N., and Jambor, J.L. (2000) Alunite-jarosite crystallography, thermodynamics and geochronology. In C.N. Alpers, J.L. Jambor and D.K. Nordstrom, Eds., Sulfate Minerals—Crystallography, Geochemistry, and Environmental Significance, 40, p. 453–479. Reviews in Mineralogy and Geochemistry, Mineralogical Society of America, Chantilly, Virginia.
Swayze, G.A., Desborough, G.A., Clark, R.N., Rye, R.O., Stoffregen, R.E., Smith, K.S., and Lowers, H.A. (2006) Detection of jarosite and alunite with hyperspectral imaging: prospects for determining their origin on Mars using orbital sensors. Workshop on Martian Sulfates as Recorders of Atmospheric-Fluid-Rock Interactions, Houston, Texas, (http://www.lpi.usra.edu/meetings/sulfates2006/pdf/7072.pdf).
Wills, A.S. and Harrison, A.H. (1996) Structure and magnetism of hydronium jarosite, a model Kagome antiferromagnet. Journal of the Chemical Society—Faraday Transactions, 92, 2161–2166.
Young, R.A. (1993) Introduction to the Rietveld method. In R.A. Young, Ed., The Rietveld Method, p. 1–38. Oxford Science Publications, U.K.

MANUSCRIPT RECEIVED JULY 4, 2007
MANUSCRIPT ACCEPTED DECEMBER 19, 2007
MANUSCRIPT HANDLED BY GEORGE LAGER